Why Modeling Particle Shape Matters

Ali, Usman; Kikumoto, Mamoru; Ciantia, Matteo Oryem; Cui, Ying; Previtali, Marco

Published in:
Journal of Geotechnical and Geoenvironmental Engineering

DOI:
10.1061/JGGEFK.GTENG-12354

Publication date:
2024

Document Version
Peer reviewed version

Why modeling particle shape matters: significance of particle-scale modeling in describing global and local granular responses

Usman Ali[1], Mamoru Kikumoto[2*], Matteo Oryem Ciantia[3], Ying Cui[4] , and Marco Previtali[5]

[1] PhD Student, Department of Civil Engineering, Yokohama National University, Tokiwadai 79, Hodogaya, Yokohama, Japan. Email: ali-usman-dp@ynu.jp

[2] Professor, Department of Civil Engineering, Yokohama National University, Tokiwadai 79, Hodogaya, Yokohama, Japan. Email: kikumoto-mamoru-fc@ynu.ac.jp

[3] Senior Lecturer, School of Science and Engineering, University of Dundee, Nethergate, Dundee DD1 4HN, Scotland, United Kingdom Email: m.o.ciantia@dundee.ac.uk

[4] Associate Professor, Department of Civil Engineering, Yokohama National University, Tokiwadai 79, Hodogaya, Yokohama, Japan. Email: sai-ei-mx@ynu.ac.jp

[5] Postdoctoral Research Assistant, School of Science and Engineering, University of Dundee, Nethergate, Dundee DD1 4HN, Scotland, United Kingdom Email: m.previtali@dundee.ac.uk

[*] Corresponding author (email: kikumoto-mamoru-fc@ynu.ac.jp)

ABSTRACT

The applicability of particle-scale modeling using the discrete element method (DEM) is typically evaluated by comparing simulation results with stress-strain responses observed in elementary tests. This validation at the global level may not guarantee that the simulation can capture realistic particle-level motion. Thus, this study investigated the applicability and limitation of two types of DEM models, through the comparison with experimental results of biaxial shearing tests on bi-disperse granular assemblies comprising circular (round) and hexagonal (angular) particles under various confining pressures. Experimental data wherein particle rotations were identified by novel image analysis technique is used to evaluate whether the DEM models could accurately reproduce macroscopic stress-strain relationships and microscopic particle responses. Experimental findings suggested that particle rotations play a crucial role in granular deformation and are influenced by the particle shape. A detailed DEM model with precise particle shapes effectively replicates both macroscopic stress-strain relationships and microscopic responses, including particle rotation and interlocking at global and local levels. Conversely, a simpler ad hoc DEM model, which incorporates rolling resistance for circular particles, can imitate the stress-strain relationships of hexagonal particles but falls short in replicating microscopic responses accurately.

Keywords: Biaxial shearing, discrete-element modeling, granular material, particle shape, particle rotation

INTRODUCTION

Granular materials comprise individual particles and voids, with the behavior of these materials being dependent on their microstructures. Understanding the micro-mechanical interactions between particles is, therefore, crucial to comprehend their macro-mechanical behavior (Andò et al. 2012; Rorato et al. 2020). Particle-scale modeling entails simulating the behavior of discrete particles within a granular system, considering actual particle shapes and establishing suitable interactions between particles to accurately replicate global and local granular responses. The Discrete Element Method (DEM) is an effective numerical approach to investigate granular behavior, allowing for the explicit simulation of individual particles (Cundall 1979; Wu et al. 2020) and particle-level motion, making it a powerful tool for studying micro-deformation mechanisms (Yimsiri and Soga 2010).

Particle shape is critical in granular systems as it governs micro-deformation mechanisms and macroscopic behavior (Shin and Santamarina 2013; Zhao et al. 2015; Nie et al. 2020; Wu et al. 2022). While circular/spherical particles have been commonly used in DEM simulations to simplify computations (Bardet and Proubet 1991; Bardet 1994; Kuhn 1999; Kuhn and Bagi 2002), these idealizations may lead to inaccurate results since natural granular materials are often non-spherical (Huang et al. 2013). For more realistic simulations, researchers have introduced elongated and angular-shaped particles (Azéma and Radjaï 2012; Azéma et al. 2012; Binaree et al. 2020; Ali et al. 2023c, 2024). Furthermore, since natural granular materials are composed of particles of various shapes, numerical experiments have been carried out by DEM with mixtures of particles of different shapes (Azéma et al. 2016; Binaree et al. 2019) and level-set DEM analyses that precisely reproduce actual particle shapes (Kawamoto et al. 2018) have also been performed. Incorporating accurate representations of soil particles in DEM simulations can be computationally demanding. Consequently, researchers have tackled this issue by introducing rolling resistance to simplified circular or spherical particles in the DEM framework (Iwashita and Oda 1998). This approach enables the consideration of deviation from realistic soil shapes while avoiding the computational complexities associated with modeling actual granular samples in DEM.

DEM models require calibration and validation as the accuracy of the numerical results depends on the selected parameters (Tong et al. 2013). The material input parameters, such as the inter-particle friction coefficient (μ) in most DEM simulations, are generally assumed or adjusted by matching stress-strain relationships, leading to values that are

often higher than the actual materials (Huang et al. 2014; Cavarretta et al. 2011). The calibration of the DEM model is typically based on the comparison with the macroscopic stress-strain response obtained from laboratory tests (Nitka and Grabowski 2021). However, these usual laboratory tests only provide a macroscopic view of the granular material response and lack microscopic particle-level information due to measurement challenges. As a result, crucial microscopic deformation mechanisms such as particle rotation are often neglected (Oda et al. 1982; Bardet 1994). Calibrating the DEM model at the macroscopic level is a common practice, but it may not be sufficient to verify particle-scale mechanisms (Tong et al. 2013; Nitka and Grabowski 2021). Thus, to ensure reliable DEM models, calibration and validation must be performed at both the particle-scale and macroscopic levels. Kawamoto et al. (2018) used an X-ray CT scan to observe particle rotation inside a sand specimen during triaxial shearing and compared the results with corresponding simulation results by a level-set DEM. They reported similar regions of predominant rotation but did not make a quantitative comparison.

To establish a comprehensive benchmark dataset for the thorough calibration and validation of the DEM from both macro and micro perspectives, this study utilizes the experimental findings obtained by Ali et al. (2021; 2023a, b) as the benchmark dataset. Ali et al. (2021; 2023a, b) performed biaxial shear tests on 2D dual-size granular assemblies consisting of around 2700 circular or 2400 hexagonal aluminum rod particles. They meticulously captured the microscopic motion of all particles using an innovative image analysis technique. These results highlighted the significance of particle rotation, a key mechanism influenced by particle shape, in determining the behavior of granular materials. The primary goal of the experiment was to establish a benchmark dataset for the comprehensive calibration and validation of the DEM, a multifaceted approach that facilitates a more precise representation of granular behavior. In this study, the authors aim to assess the validity of two recent popular DEM approaches for capturing the macro as well as microscopic behavior of noncircular particles. The first approach involves using Hertz-Mindlin contact theory with direct modeling of realistic shapes, while the second approach incorporates linear contact theory with the addition of rotation constraints (rolling resistance) to circular particles to emulate the behavior of noncircular particles. For this, the authors developed two types of 2D DEM models to simulate biaxial shear tests and compared their ability to replicate the microscopic particle-level motions and macroscopic stress-strain characteristics observed in the experiments. The first

model was a detailed one that accurately represented particle characteristics and material properties. To minimize discrepancies between the experiment and simulation, this model incorporated particle shape, particle size distribution, and constants such as friction coefficient determined uniquely from laboratory tests. The primary objective of this detailed DEM model was to assess the extent to which a sophisticated DEM could replicate realistic phenomena. The second model is a simple ad hoc model designed to mimic the response of noncircular particles using circular particles with artificial rolling resistance. Given the difficulty in modeling the actual particle properties of granular materials, which typically have particles with different shapes, and the simplicity and low computational cost, this model has been widely used. The model simulated the response of regular hexagonal particles using a DEM of a circular particle with rolling resistance, and the study discussed the limitations of this ad hoc model.

OUTLINE OF BIAXIAL TESTS

Biaxial test apparatus

Fig. 1 depicts the schematic illustration of the apparatus utilized in the present study. A square sample box, featuring rigid boundaries, was employed with dimensions of 350 mm x 350 mm and a wall thickness/depth of 50 mm. The bottom wall was fixed, while the top and side walls were only permitted to displace normally. Both the front and back sides of the sample box were left open, enabling the recording and visualizing deformation of the granular assembly during the test. Load and displacement measurements were taken in both axial and lateral directions. Load control in the lateral direction was achieved through a pneumatic cylinder, while control in the axial direction could be executed via either load control with a pneumatic cylinder or displacement control with an electric jack. A displacement transducer was employed to determine the relative lateral displacement of the side walls, while the axial displacement was obtained by averaging the measurements of the right and left ends of the top wall taken by two displacement transducers. Lateral and axial strains were obtained by dividing lateral and axial relative displacements by the initial width and height of the specimen, respectively. The axial load was obtained by averaging the readings of two load cells installed at the top and bottom walls, and the lateral load was measured through a load cell installed at the right wall. A data logger was utilized to measure the displacements and loads in axial and lateral directions, with data being collected by a computer. Axial and lateral stresses were calculated by dividing the respective loads by the cross-sectional areas of the specimen perpendicular to each

direction, with cross-sectional areas continuously updated based on the measured lateral and axial displacements. For strain-controlled loading in the axial direction, the axial strain rate (i.e., 0.014% per sec) was regulated by applying a prescribed displacement rate to the cylinder rod via an electric jack. The axial strain rate was selected to ensure the quasi-static shearing process. For stress-controlled loading in the lateral direction, lateral stresses were monitored by the computer and controlled through the modulation of air pressure to the pneumatic cylinder II. The PC regulated the air pressure applied to the pneumatic cylinder by sending prescribed voltage signals to electro-pneumatic regulators through a digital analog board. The tests were conducted at three different confining pressures (σ_3), namely 19.6kPa, 39.2kPa, and 58.8kPa.

The utilization of aluminum rods is widely acknowledged in the study of granular materials under two-dimensional, plane strain conditions (Schneebeli 1956). The experimental setup comprises dual-sized circular rods of diameters 10 mm and 6 mm, and hexagonal rods with inscribed diameters of 10 mm and 6 mm, all with a uniform length of 50 mm, corresponding to the depth of the biaxial sample box. It should be noted that, due to material availability constraints, the diameter of the circular rods matches the inscribed diameter of the hexagons. Consequently, the cross-sectional area of the hexagon rod is approximately 10% larger than that of the corresponding disc. This discrepancy in the area leads to a situation where fewer hexagon rods are needed to fill the biaxial box compared to circular rods. The material can stand without any support on the front and back sides and achieve the plane strain condition. The mixing ratio of big to small particles is 2:3 by weight. The material density of the aluminum rods is 2830 kg/m^3. Further details about the experimental setup can be found in Ali et al. (2023a). Fig. 2 shows the shapes and sizes of aluminum rods used in the experiment.

In the biaxial test, σ_1 and σ_3 represent the major and minor principal stress values in the *y* and *x* directions, respectively. The mean stress and deviatoric stress are expressed as $\sigma_n = (\sigma_1+\sigma_3)/2$ and $\sigma_s = \sigma_1 - \sigma_3$, respectively. ε_1 and ε_3 represent the major and minor principal strain values in the *y* and *x* directions, respectively. The volumetric and deviatoric strains are expressed as $\varepsilon_n = \varepsilon_1 + \varepsilon_3$ and $\varepsilon_s = \varepsilon_1 - \varepsilon_3$, respectively.

Image analysis process

The image analysis process comprises several sequential stages, including the preparation of surface-treated specimens,

image acquisition, particle identification, tracking, and rotation detection. The surface of the specimens is treated in a way that enhances image analysis quality by capturing high-resolution images. For this, circular black stickers bearing two red and green dots are affixed to each particle. These dots on the dark circular background facilitate the identification of the particles' geometric transformations. During the shearing test, digital images are acquired every 20-25 seconds intervals using a PENTAX K3 II camera, 24.35 megapixels (6016 x 4000). The images are then processed to enhance their quality by adjusting the intensity and applying other image adjustment techniques to improve the accuracy of image analysis. The widely utilized "imfindcircles" function within MATLAB is employed to identify circular objects in images and determine the centroids and radii of particles. Particle translations are tracked using an algorithm developed by Crocker and Grier (1996). The trajectories reflect only the particles' translational movements, excluding any rotational movements. Thus, the Multiscale Analysis for Granular Image Correlation algorithm developed by Chen et al. (2017) is applied to estimate particle rotations. The accuracy of the rotation algorithm was assessed prior to implementation. Rotation estimation during the biaxial test is performed by correlating two consecutive images taken during the test. Further details about the image analysis process can be found in Ali et al. (2023b).

OUTLINE OF DISCRETE ELEMENT SIMULATION

A numerical simulation tool, "Particle Flow Code (PFC)," developed by Itasca Consulting Group Inc., has emerged as a practical Discrete Element Method (DEM) framework. Typically, PFC provides a platform for users to create codes that address a range of DEM problems (Ciantia et al. 2019; Nie et al. 2020; Wu et al. 2021). In this study, simulations were performed using the software PFC2D 7.0.

Biaxial shear tests were simulated at the same scale, utilizing a square sample box of 350 mm x 350 mm side length, as utilized in the experiments. The granular samples are generated with the radius expansion method. The required number of particles were placed in the biaxial box with their sizes smaller than the actual sizes, subsequently, the particles underwent expansion to their actual dimensions. During expansion, rigid wall boundaries were servo-controlled, interparticle friction was set to zero, and the sample was cycled until an equilibrated state with the desired porosity was achieved. The simulations were performed in two phases: (a) isotropic compression was carried out by incrementing the confining pressure, resulting in the normal movement of the right and top walls, with the condition of $\sigma_1 = \sigma_3$; in contrast,

the left and bottom walls of the biaxial chamber were fixed (b) the shearing test was then performed at constant confining pressure, with the top wall moving downward normally under the loading condition of $\sigma_1 > \sigma_3$. The axial strain rate during shearing was 0.05% per sec, ensuring quasi-static shearing. The shearing test was performed with each shape at three different confining pressures σ_3 = 19.6, 39.2, and 58.8 kPa.

Two types of 2D DEM models were developed: the first model was a detailed one that incorporated circular and hexagonal particle shapes, particle size distribution, and material constants precisely; the second model is a simplified model containing only circular particles, and rolling resistance is applied to these circular particles to mimic the hexagonal particles response.

Detailed DEM model incorporating particle shape

The first detailed DEM model incorporated circular and hexagonal samples of the same shape and size as used in the experiment. The particle size distribution, initial void ratio, and other conditions were identical to the experiments. Fig. 3 depicts the initial states of the DEM model of bi-disperse circular and hexagonal disks. Fig 4 presents a comparison between the contact normal fabrics of the test samples detected from photos and the equivalent DEM samples. This comparison shows that the initial fabric condition indicates an isotropic state in both the experiment and simulation. This is primarily a result of employing non-elongated particles (Ali et al. 2024). Consequently, the experiment and simulation exhibit reasonable repeatability, with no significant effects stemming from the initial fabric state. The Hertz contact model based on the theory of Mindlin and Deresiewicz (1953) is used for the particle–particle and particle–wall interactions. It can produce both normal and shear forces based on the theoretical analysis of the deformation of smooth elastic spheres in frictional contact. The material parameters for the simulation are based on aluminum, as the reference experiment involved the use of aluminum particles. Material parameters summarized in Table 1 are applied as the parameters for the particles. The interparticle friction coefficient was measured by performing a direct shear test with two aluminum disks. As the walls of the biaxial box are also made of aluminum material, therefore, reproducing laboratory test boundary conditions is important to have a quantitative agreement between the response observed in the simulation and laboratory tests (Cui et al. 2007). Hence, wall stiffness and surface friction are assigned to be the same as that of the particle to reproduce laboratory test boundary conditions. By fixing all material parameters, the value of shear modulus (G) was

precisely calibrated by simulating and matching the response of circular particles with corresponding experimental data.

Simplified DEM model using circular particles with rolling resistance

The use of common particle shapes in DEM, such as discs or spheres, can lead to inaccurate results because they differ significantly from the actual shape of real soils (Huang et al. 2013). To address this issue while avoiding the computational complexity of replicating actual granular samples in DEM, researchers often apply rolling resistance to circular or spherical particles in DEM to account for the deviation from realistic soil shapes (Iwashita and Oda 1998). Recent research has investigated the effect of adding rotation constraints to circular samples on the mechanical response of granular systems (Bardet 1994; Zhang et al. 2013) and compared it with the response of different shapes such as clumps (Wensrich et al. 2014) and regular polygons (Estrada et al. 2011). Initially, rolling resistance was calibrated to imitate certain shapes by matching macroscopic responses. However, to effectively solve the calibration problem, researchers have tried to link particle shape and rolling resistance quantitatively. For example, Estrada et al. (2011) theoretically calculated rolling resistance for ideal regular 2D polygons, while Rorato et al. (2021) suggested that using the physical measure of particle sphericity of real sand grains to calibrate rolling resistance through a detailed comparison of identical experimental and numerical tests would be a better approach. As the shape of real grains is very complex and often described by multiple independent shape descriptors, mainly sphericity, angularity, and roughness (Mitchell and Soga 2005), studies on the effect of particle shape revealed that each shape descriptor has its effect on the mechanical response of the granular system (Rothenburg and Bathurst 1992; Mirghasemi et al. 2002). Therefore, the application and calibration of rolling resistance to imitate complex shapes remain a hot topic in research.

Consequently, a simplified second DEM model was developed, employing conventional 2D circular particles with artificially incorporated rolling resistance to mimic the experimental response of circular and hexagonal particles. The initial conditions such as particle size distributions, void ratios, and other pertinent testing conditions of the circular samples were kept the same as the circular sample used in the experiment. The primary aim of this model is to ascertain whether the rolling resistance approach is reasonable for emulating both macroscopic and microscopic responses observed in noncircular particles. The contacts among particles and between particles and walls are described using a rolling resistance linear contact model available in the commercial DEM software PFC2D 7.0. The rolling resistance linear model

builds upon the conventional linear elastic frictional contact model, to which a rolling-resistance (μ_r) mechanism is introduced (Iwashita and Oda 1998; Rorato et al. 2021).

To calibrate the second DEM model, an initial step involved simulating the response of circular particles response without applying rolling resistance and comparing these simulations with experimental results for circular particles. Throughout the calibration process, meticulous efforts were undertaken to maintain consistency in the input parameters, including the utilization of the same material (aluminum) and simulation parameters as employed in the detailed DEM model described earlier. However, special attention was paid to fine-tuning the value of effective normal contact stiffness (*Emod*) to ensure alignment with corresponding experimental data. Table 2 shows the final sets of material parameters used for the second DEM model. The value of the rolling resistance for a regular hexagon on a flat horizontal surface was theoretically calculated to be around 0.137 or 0.134 (Huang et al. 2013; Estrada et al. 2011). However, in our experimental setup, a bi-disperse mixture was utilized to avoid the tessellation effect of mono-sized regular hexagons. Therefore, the value of rolling resistance assigned to circular particles to imitate hexagonal particles was then carefully calibrated by trial-and-error method by matching with the stress-strain response of the hexagons observed in the experiment. After achieving a good agreement between macroscopic responses, the authors compared microscopic responses such as particle rotation to investigate whether the particle-level behavior could also be reasonably captured.

BIAXIAL TEST RESULTS

In our previous publication (Ali et al. 2023a,b), we extensively discussed the responses of bi-dispersed circular and hexagonal rods in biaxial shearing tests. Our findings revealed that hexagonal particles, characterized by their angular shapes, exhibited significantly higher shear strengths when compared to circular particles. The increased strength observed in hexagonal assemblies was attributed to reduced rotations, resulting from the stronger interlocking between angular particles. In contrast, circular particles displayed lower macroscopic strengths because they were more susceptible to significant rotations during shearing, primarily due to the absence of substantial interlocking. For a detailed comparison of macro and microscopic experimental responses of circular and hexagonal particles, see Ali et al. (2023a).

The primary aim of this paper is to compare the experimental results involving circular and hexagonal particles

with two distinct DEM models: the first model accurately represents the actual particle shape, while the second model employs circular particles and imitates hexagonal particles through the introduction of rolling resistance. This study seeks to emphasize the importance of precise modeling of particle shapes in DEM and outline the practical applicability and limitations of using circular particles enhanced with rolling resistance. Firstly, the subsequent section 5 presents a thorough comparison of simulation results obtained from the detailed DEM model utilizing Hertz-Mindlin contact theory, which incorporates actual particle shapes. Following that, in section 6, a comprehensive comparison is provided between the experimental and simulation results from the simplified DEM model, wherein linear contact theory is applied, and rolling resistance is added to circular particles to imitate the experimental response of hexagonal particles.

VALIDATION OF DETAILED DEM MODEL

The initial calibration of the detailed DEM model involves conducting simulations with circular particles and comparing the results against a comprehensive set of experimental data obtained from circular rods. Following this calibration, the validation of the DEM model takes place by altering the particle shape from circular to hexagonal. The numerical results are then compared against the corresponding experimental data obtained from hexagonal particles.

Comparison of macroscopic behavior

Fig. 5 illustrates the stress-strain relationships (σ_1/σ_3 - ε_s) and volumetric deformations (ε_n - ε_s) of circular and hexagon samples observed in both the experiment and simulation under three different confining pressures. The DEM model reasonably captures the effect of shape on the stress-strain response observed in the experiment quantitatively. In the experimental study, hexagon samples exhibit a higher critical state strength and a larger dilation. A similar trend is also observed in the simulations. For hexagonal particles, the simulation results adequately capture the impact of particle shape on critical state strength. However, they do not entirely reflect the stiffness observed during the initial shear stage, as indicated by the experimental observations. The volumetric behavior in the experiment exhibits a pronounced dilatancy under lower confining pressure, which is similarly observed in the numerical simulations.

Fig. 6 shows the relationship between the mean stress (σ_n) and critical state stress ratio $(\sigma_1/\sigma_3)_{cs}$. The average critical state stress ratio obtained from three different confining pressures for circular samples in the experiment and simulation is 1.80 and 1.76, respectively, while for hexagon samples in the experiment and simulation, it is 2.54 and 2.52,

respectively indicating that the critical state strength of the hexagonal (angular) samples becomes significantly higher. Similar variation in critical state stress ratio is observed in the experiment and simulation, and the simulation results are reasonably close to the experimental data.

Comparison of microscopic behavior

Fig. 7 portrays the history of absolute average cumulative rotation (r_m) for particles in the complete assembly observed in the experiment and simulation.

$$r_m = \frac{\sum_{i=1}^{N}|\theta_i|}{N} \tag{1}$$

where θ_i is the cumulative rotation of an individual particle i, and N is the total number of particles in the sample. The experiment reveals that the r_m for circular and hexagonal samples, upon completion of shearing ($\varepsilon_s \approx 20\%$), is 18.6° and 9.7° respectively, indicating that a circular particle undergoes approximately twice as many rotations as a hexagonal particle. The simulation also shows that, on average, circular particles rotate almost twice as much as hexagonal particles, with the r_m at the end of shearing being 21.6° and 10.5° for circular and hexagonal samples, respectively. The detailed DEM model with appropriate parameters calibration is capable of quantifying the particle-scale behavioral changes in granular samples that are contingent upon particle shape.

Histograms in Fig. 8 depict the density distribution of cumulative rotations for each particle from initial to final orientations during shearing. Fig. 8(a) depicts the density distribution of cumulative rotation for circular and hexagonal particles at the end of shearing observed in the experiment. Rotations are found to be normally distributed in both clockwise and counterclockwise directions around a mean value of zero degrees, a phenomenon similarly observed by various researchers (Oda et al. 1982; Misra and Jiang 1997). Experimental results indicate that circular particles tend to rotate more readily than hexagonal particles. The histogram of the rotation density distribution highlights a higher concentration of hexagonal particles around the mean value, suggesting that a greater proportion of these particles refrain from rotation within the hexagonal assemblies. Fig. 8(b) presents an equivalent plot of simulation results. The rotational behavior of both shape assemblies in the simulation follows a normal distribution, consistent with the experimental observations. The simulation captures the influence of particle shape on rotational behavior, displaying a comparable difference in the rotational behavior of hexagonal and circular particles. It is typically observed that rotation in one

direction is frequently accompanied by a nearly equivalent opposing rotation in the immediate or far neighboring region, leading to the formation of clusters of particles exhibiting rotations in a similar direction. This was similarly observed by Kuhn and Bagi (2002) in their investigation of rotation clusters within biaxial assemblies of circular particles. The formation of rotation clusters is more prevalent in angular samples, owing to the stronger interlocking between particles.

Shear bands and particle rotation

Elementary tests, such as biaxial tests, presume a uniform elementary response of the specimen, however, shear bands tend to develop with strain localization near failure. The shear bands govern the overall response at failure, determining the macroscopic strength. In dense samples, which tend to dilate when sheared, the local void ratio within the shear band increases more rapidly, and the coordination number decreases compared to other parts of the sample (Mitchell and Soga 2005). Furthermore, significant particle rotations tend to concentrate inside the shear band, resulting in rotation localization (Iwashita and Oda 1998; Rorato et al. 2020; Ali et al. 2023b). Hence, it is essential to investigate the behavior of particles inside the shear band.

A nominal deviatoric strain is assigned to each particle using a procedure developed for the DEM post-processing technique by Catalano et al. (2014), and the particles inside the shear band are identified. In this procedure, Voronoi cells with the particles' mass centers as nodes are created using a regular Delaunay triangulation available within YADE (Smilauer et al. 2015). Thus, the particle positions at two instants towards the end of shearing (for example, when ε_s is 16 % and 20 %) were identified, and nodal displacements were introduced in YADE. Displacements were then differentiated partially to the spatial coordinates to obtain displacement gradient tensors for the triangles. A nominal averaged deviatoric strain was finally projected back to each particle, and a threshold deviatoric strain value of 5 % was applied to assign particles to the shear band. The same procedure was applied to identify the particles inside the shear bands in the triaxial tests on sands by Rorato et al. (2020). The particles inside the shear band are represented as black particles in Fig. 9. In the experiment, two X-shape shear bands were observed along the diagonals of the biaxial box in each sample, due to rigid boundary conditions. The simulation results also showed the formation of similar two X-shape shear bands, indicating that the DEM model is able to identify non-uniform deformation zones. Fig. 10 demonstrates the absolute average cumulative rotation (r_m) of particles inside and outside the shear band for both circular and hexagonal

samples in the experiment and simulation. Particles inside the shear zone tend to have a greater magnitude of rotation from the initial shear stage. This results in the localization of particle rotations, leading to the localization of deformation and the formation of shear bands. The comparison of rotational behavior between particles inside and outside the shear band indicates that the DEM model could reasonably capture the granular behavior, even in a non-uniform deformation regime. For instance, the r_m inside the shear band at the end of shearing ($\varepsilon_s \approx 20$ %) for circular particles was 26.6 ° in the experiment and 29.2 ° in the simulation. Similarly, the r_m inside the shear band for hexagonal particles was 11.9 ° in the experiment and 15.8 ° in the simulation.

Effect of particle size

Fig. 11 presents the density distribution histograms of cumulative particle rotations observed in the experiment and simulation based on the particle sizes. For circular particles, a clear difference in rotation magnitude between small and big particles is observed. However, distributions for both sizes follow a symmetric distribution around a mean value of approximately 0 °. The rotation of small circular particles is significantly greater than that of big particles. The absolute average cumulative rotation ratio of small circular particles to larger ones is 1.7 and 1.8 in the experiment and simulation, respectively, indicating that small particles rotate nearly twice as much as big particles in both cases. This difference results in a ball-bearing effect, where small circular particles act as ball-bearings between the big particles, leading to a reduction in strength. Vallejo (2001) also observed a similar effect of small particles in dual-size circular mixtures. In contrast, for hexagonal particles, there is no significant difference in the rotation of small and big particles observed in both experiments and simulations, indicating stronger interlocking between hexagonal particles. The absolute average cumulative rotation ratio observed for the small to big hexagonal particles is 1.1 and 1.3 in the experiment and simulation, respectively. Therefore, it can be concluded that particle size has a significant effect in circular samples, while its effect is insignificant in hexagonal samples, which is also observed in the simulations.

Effect of confining pressure

Fig. 12 shows the cumulative particle rotations density distribution histograms for circular particles plotted for three different confining pressures for both the experiment and simulation. The rotational behavior of circular particles is not significantly affected by the confining pressure, as observed in both the experiment and simulation results. The effect of

confining pressure on the rotational behavior of particles is insignificant. The effect of confining pressure remains consistent for hexagonal particles.

VALIDATION OF THE SIMPLIFIED DEM MODEL WITH ROLLING RESISTANCE

Initially, the simplified DEM model is employed to simulate the behavior of circular particles without considering rolling resistance. Since the experimental particles were perfectly circular, ensuring no disparity between the particles' shape in the experiment and simulation, the DEM model theoretically should accurately represent the response without incorporating rolling resistance. To calibrate the simplified DEM model, numerical results are compared against experimental data for circular particles. Upon successful calibration, the next step involves introducing rolling resistance to circular particles. This is done with the aim of capturing the experimental response of hexagonal particles.

Predicting circular response with no rolling resistance

In Fig. 13, the stress-strain and volumetric responses of circular particles are compared between the experimental observations and simulations using the simplified DEM model with no rolling resistance applied under three different confining pressures. The results indicate that the DEM model, employing a linear elastic frictional contact model, is capable of replicating the behavior of circular particles. In the experiment, the circular particles demonstrate an average critical state stress ratio of 1.80, while the simulation yields a very close ratio of 1.83 for all confining pressures. Furthermore, the volumetric response is reasonably well captured, with a slight compression phase followed by a dilative response, and ultimately, the specimen undergoes shearing without any significant change in volumetric strain. The dilations tend to be more obvious under low confining pressures.

Fig. 14 presents a comparison of the absolute average cumulative rotation (r_m) within and outside the shear bands for the case of σ_3 = 39.2kPa. Interestingly, the simple DEM model demonstrates the ability to effectively capture the overall rotational behavior of the circular particles at the particle level. In the experiment, the r_m value of total particles at the end of shearing amounts to 18.6°, while in the simulation, it is 22.1°, a value quite close to the experimental result. Moreover, within the experiment, the r_m values at the end of shearing inside and outside the shear band are 26.6° and 15.4° respectively, while in the simulation, they are 32.6° and 15.1° respectively. This comparison indicates that the developed simplified DEM model can reasonably reproduce the experimental response of circular particles, both at the

macro and microscopic levels.

Furthermore, Rorato et al. (2021) conducted 3D DEM simulations to calibrate rolling resistance and reproduce realistic sands' triaxial response. Their findings indicated that even if the sand particles were perfectly spherical with a unit 3D sphericity value, a rolling resistance of 0.2 was still necessary to accurately mimic the realistic response in DEM. This requirement stems from the fact that real sands comprise particles with varying shapes, and although a majority may be spherical, there exists a range of sphericities among the grains. Consequently, a simple DEM model employing only spherical balls cannot entirely represent a realistic sand specimen without some rolling resistance to account for the shape differences, even for spherical sands. However, in our study, the utilization of high-quality biaxial experiments with perfectly circular particles allowed for precise replication of the specimen in the DEM model, eliminating any discrepancies. The results from our study, specifically within the 2D granular system, suggest that no rolling resistance is needed to accurately imitate the response of circular particles. After successfully calibrating the simplified DEM model, rolling resistance is introduced to circular particles to replicate the experimental response of hexagonal particles. Besides indirectly replicating hexagonal responses through rolling resistance, the calibrated linear spring contact model was also directly utilized to simulate hexagonal-shaped particles. Our findings suggested that employing the linear model for the direct simulation of hexagonal-shaped particles tends to slightly overestimate shear strengths. However, it accurately reproduces the rotational behavior of hexagonal particles both inside and outside the shear band. Further details about the results of these simulations and their comparison with equivalent experiments are elaborated in Appendix A.

Imitating hexagonal response using rolling resistance

To imitate the experimental response of hexagonal rods, a DEM model with circular particles with the same inscribed diameters as that of hexagons is employed, wherein the rotation of circular particles is restricted by adding rolling resistance within the linear contact model framework. As mentioned earlier, the initial contact normal based fabric of the experimental hexagonal samples demonstrates relatively isotropic conditions at the beginning of the shearing. Similarly, the corresponding DEM model, employing circular particles to replicate the experimental response of hexagons, also depicts an isotropic fabric state of contact normals at the start of shearing (as shown in Fig 4).

Different values of rolling resistance were applied to the circular particles, and numerical results were compared with the experimental response of hexagonal particles. Based on the trial-and-error method, a value of rolling resistance showing a reasonable match with the hexagon experiment was selected. The results suggest that applying a rolling resistance of 0.2 to circular particles in the simulation can reasonably replicate the macroscopic behavior of hexagonal particles, particularly critical state shear strengths. The value of rolling resistance selected is quite close to the theoretical values recommended by Huang et al. (2013) and Estrada et al. (2011) for 2D regular hexagons. Fig. 15 shows the comparison between the macroscopic stress-strain response of hexagonal particles observed in the experiment and circular particles with rolling resistance under three different confining pressures. Specifically, the average critical state stress ratio for all the experiments depicted in Fig. 15 is 2.54, which is reduced to 2.49 upon replication by applying rolling resistance to circular particles in the simulation.

Subsequently, microscopic behavior was assessed by comparing particle rotations, and Fig. 16 illustrates the evolution of the absolute average cumulative rotation (r_m) within and outside the shear bands for the case of σ_3 = 39.2kPa. Despite the good agreement achieved in terms of macroscopic response, a difference in the rotational behavior of the particles was observed microscopically, with the magnitude of the difference being higher outside the shear band. However, when actual hexagonal shape particles were modeled in simulations, the rotational behavior closely predicted experimental results, as demonstrated in Fig 10(c) and 10(d).

Furthermore, Fig. 16(a) indicates that the rotational behavior of hexagonal particles is similar in the initial stage of shearing, with the rotations tending to concentrate inside the shear band when ε_s reach 5%. This suggests that angular particles interlock more effectively and that a certain degree of shearing is required for rotations to concentrate within the shear band. This observation is consistent with the behavior of actual hexagonal particles, as demonstrated in Fig. 10(d). In contrast, a clear difference was observed for circular particles with rolling resistance from the start of shearing, as shown in Fig 16(b), indicating a relatively weaker interlocking state than actual hexagon particles.

Thus, it can be inferred that validation of DEM models with the application of rolling resistance is suitable only for reproducing macroscopic behavior (as shown in Fig. 17) while slightly compromising the particle-level mechanisms. Therefore, when employing DEM models to investigate micro-deformation mechanisms in granular systems, it is crucial

to model actual shapes and validate the models by comparing them with at least two datasets of the different shapes.

Interlocking is a resistance mechanism that results from the particle arrangement of granular materials, and it is considered an important source of shear strength (Liu et al. 2023). Fig. 18 presents the arrangement of hexagonal particles at different strain levels during shearing in the detailed DEM model with hexagonal particles applied in the previous section. At the onset of shearing, initial compression leads to a well-packed arrangement of hexagonal particles, resulting in a strong interlocking between the particles, as illustrated in Fig. 18(a) and (b). Angular particles exhibit fewer rotations due to the stronger interlocking. As shearing continues and dilation begins, particles override each other, leading to the weakening of the interlocking, as illustrated in Fig. 18(c). Finally, rotation concentrates inside the shear band, as shown in Fig. 10(d). However, the simplified DEM model that utilized circular particles with rolling resistance did not show this kind of evolution of particle arrangements observed in angular particles (as shown in Fig. 19). This is because, even if rolling resistance is applied to circular particles, the spatial rearrangement of angular particles encouraging interlocking never happens. Huo et al. (2023) also reported similar findings, highlighting that the particle shapes cannot be adequately substituted using sphere models and rolling resistance due to intrinsic differences in their micro-mechanics.

CONCLUSIONS:

This study had two main objectives: (1) to verify the reliability of the detailed DEM model that incorporates actual particle shapes and material properties by comparing it with equivalent experimental data on circular and hexagonal particles at both macroscopic and microscopic levels, such as stress-strain characteristics and particle rotations, respectively; and (2) to highlight the potentials and constraints of the simplified ad hoc DEM model using circular particles with rolling resistance in imitating the macro and microscopic response of non-circular particles.

The study conducted biaxial shearing tests on dual-size granular assemblies comprising circular or hexagonal particles, in both experiments and DEM simulations. A new image analysis was carried out to capture particle rotations. The detailed DEM model results were compared with two experimental datasets to assess its ability to include particle shape effects on granular material behavior at both macroscopic and microscopic levels, including stress-strain characteristics and particle rotations, respectively. The results showed that the detailed DEM model, especially when employing a Hertz-Mindlin contact model, was effective in capturing the impact of particle shape on both macroscopic

stress-strain response and particle-level rotational behavior during shearing. The simulation also identified similar non-uniform deformation zones or shear bands as observed in the experiments, and the particle behavior in the shear bands was accurately captured. Furthermore, the DEM model could reasonably represent the effect of particle size and confining pressure on rotational behavior in dual-size samples.

A DEM model using linear elastic contact theory with a rolling resistance mechanism was further used to simulate the biaxial shearing tests, where circular particles with artificial rolling resistance were used to replicate noncircular particles. The conclusion drawn is that when employing linear elastic contact theory, there is no need for rolling resistance to accurately replicate the experimental response of circular particles. However, rolling resistance becomes necessary only when the DEM-generated specimen deviates in shape from the reference experimental specimen. The use of circular or spherical shapes with rolling resistance in DEM is not enough to replicate the behavior of non-circular or non-spherical particles, especially on a particle-level mechanism such as interlocking and rotations, although it can capture the macroscopic response by adjusting the rolling resistance. Therefore, this study emphasizes that for verifying the reliability of DEM models in accurately capturing realistic granular behavior, a comprehensive calibration procedure must be employed, which includes a comparison of numerical and experimental results at both macroscopic and microscopic levels. Additionally, when conducting parametric studies, such as using multiple particle shapes in the simulation, it is reasonable to compare the DEM with more than one experimental dataset to further verify its validity.

Furthermore, the particle-scale modeling approaches examined in this study emphasizes the significance of precisely modeling particle shapes and selecting appropriate contact models to accurately reproduce realistic global and local granular responses.

ACKNOWLEDGMENTS

The Ministry of Education, Culture, Sports, Science and Technology of Japan is acknowledged for giving financial assistance through MEXT scholarship to the first author to study at Yokohama National University, Japan. This work was funded by JSPS KAKENHI under grants 24360192 and 19H00780 to the corresponding author. We also gratefully acknowledge the financial support from the Royal Society International Exchanges research grant (IES/R1/201238) for the 2nd and 3rd authors.

DATA AVAILABILITY

The datasets generated during and analyzed during the study are available from the corresponding author upon reasonable request.

APPENDIX A: HEXAGONAL RESPONSE WITH LINEAR SPRING MODEL

Fig. A1 displays the comparison of stress-strain and volumetric responses of hexagon shaped particles observed in both the experiment and DEM simulation using linear spring contact model. Overall, there is a clear similarity between the response observed with the linear spring contact model simulation and the experimental findings. In experiments, the average critical state stress ratio across all three confining pressures was 2.54 and, in the simulation, employing the linear spring contact model, this average was 2.80. Meanwhile, when using the Hertz Mindlin contact model, the same average was 2.52, indicates that the linear spring contact model tends to slightly overestimate the shear strengths. This suggests that while the linear contact model performs effectively for circular discs, it tends to slightly overestimate shear strengths for angular particles. As a result, it can be inferred that the shear response of angular particles observed through the Hertz contact model aligns relatively closer to the corresponding experimental response compared to the linear spring contact model.

Fig. A2 illustrates the progression of the absolute average cumulative rotation of particles for the entire sample, both inside and outside the shear band for the case of σ_3 = 39.2kPa. It is vital to highlight that employing the genuine hexagonal shape, even with the linear spring contact model, can effectively reproduce the rotational behavior of hexagonal particles. Similar to the experimental findings, the rotations at the initial stages of shearing demonstrate a close resemblance, and as shearing progresses, the rotations tend to concentrate within the shear band. This mechanism is associated with the interlocking characteristics inherent in hexagonal-shaped particles, as discussed earlier. This observation further emphasizes the importance of modeling the actual particle shape and highlights the limitations of employing a rolling resistance approach in accurately predicting the microscopic response of particles during granular shearing.

FIGURES AND TABLES

Table 1. Material parameters for detailed DEM model (Hertz contact model)

Description	value
Mass density [kg/m^3]	2710
Coefficient of friction, μ	0.20
Shear Modulus, G [GPa]	26.0
Poisson's ratio, v	0.30
Local damping parameter	0.20
Inertial number, I (10^{-7})	0.7-2.2

Table 2. Material parameters for simplified DEM model (rolling resistance linear contact model)

Description	value
Mass density [kg/m^3]	2710
Coefficient of friction, μ	0.20
Effective normal contact stiffness, *Emod* [Pa]	2e7
Normal-to-shear stiffness ratio, *kratio*	2.0
Local damping parameter	0.20
Inertial number, I (10^{-7})	0.7-2.2
Rolling resistance, μ_r	0 and 0.2

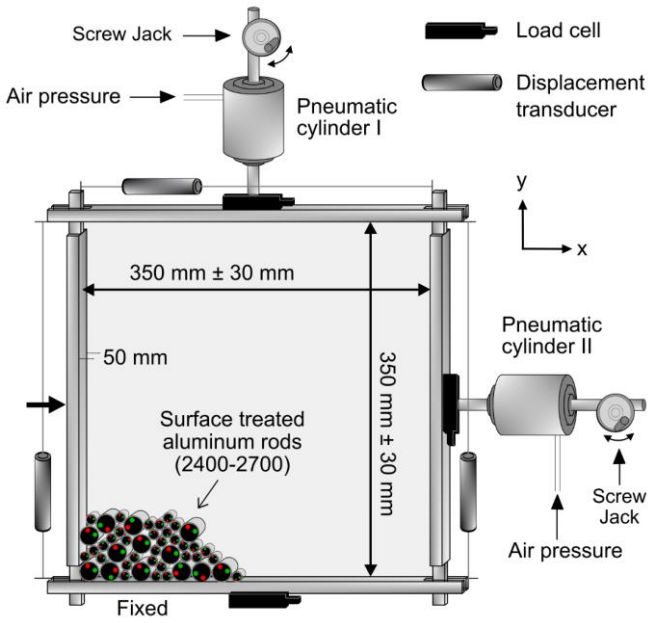

Figure 1. A schematic view of the biaxial test apparatus (front side)

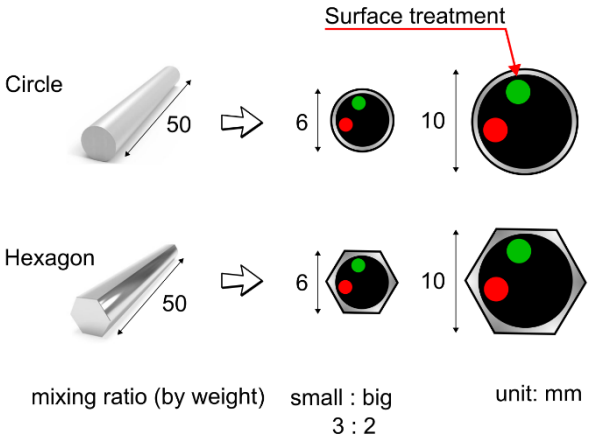

Figure 2. Shapes and sizes of aluminum rods used in the biaxial shearing experiment

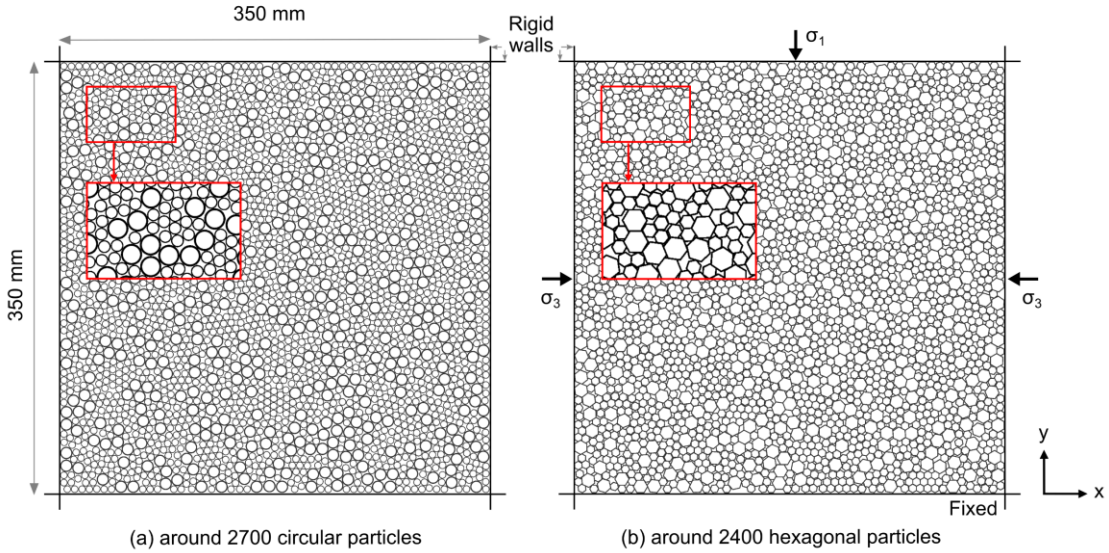

Figure 3. Discrete element model of biaxial shear test (a) circular assembly used for calibration of both DEM model with different contact methods (b) hexagon assembly used for validation of detailed DEM model and shearing mechanism

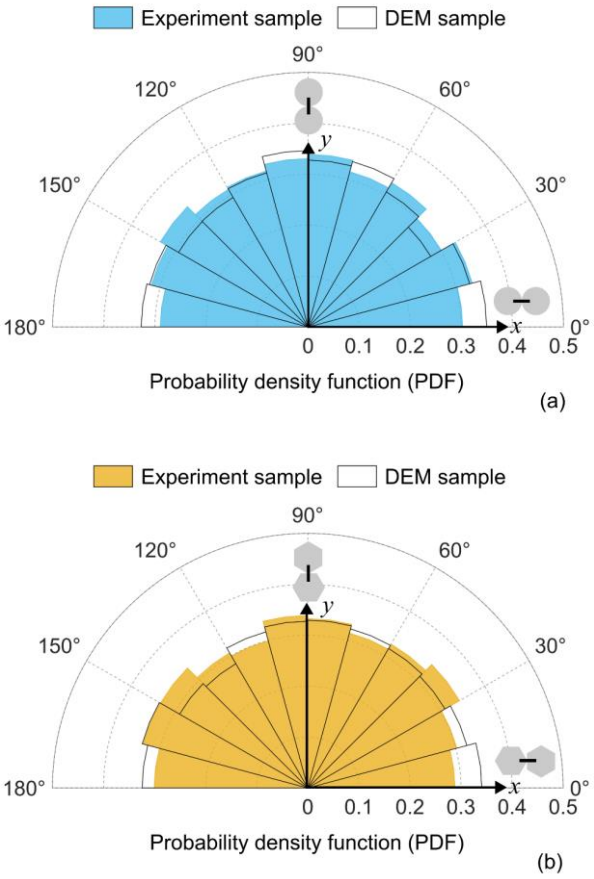

Figure 4. Polar histograms showing comparisons of contact normal orientations in experimental samples and corresponding DEM simulation samples (a) Circular particles (b) Hexagonal particles

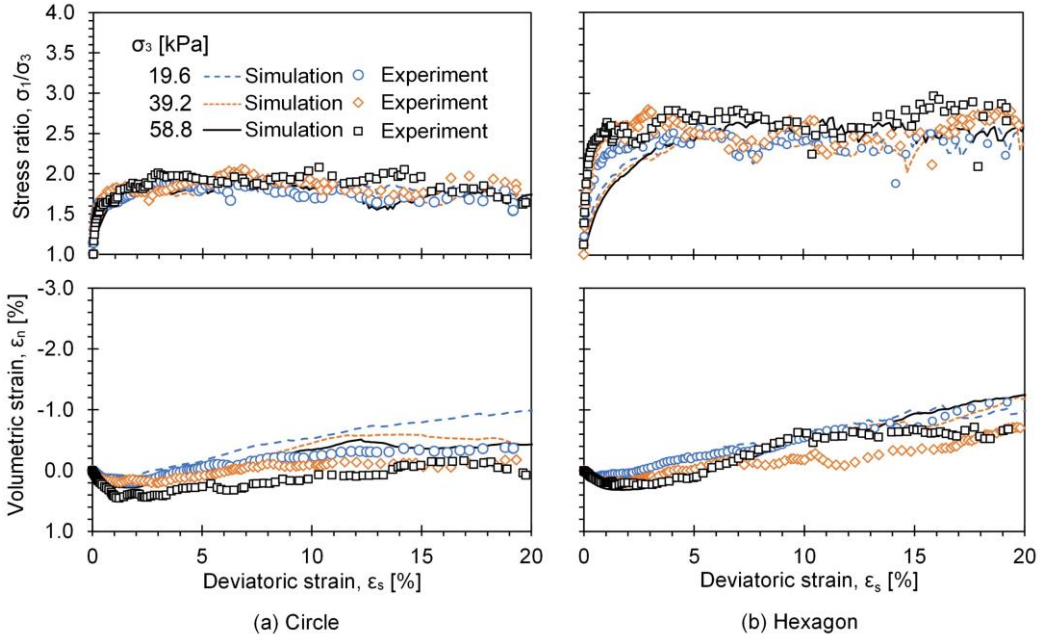

Figure 5. Stress-strain relationship and volumetric behavior of 2D disks observed in experiment and DEM simulation (Hertz-Mindlin contact model) under three different confining pressures (a) circle (b) hexagon

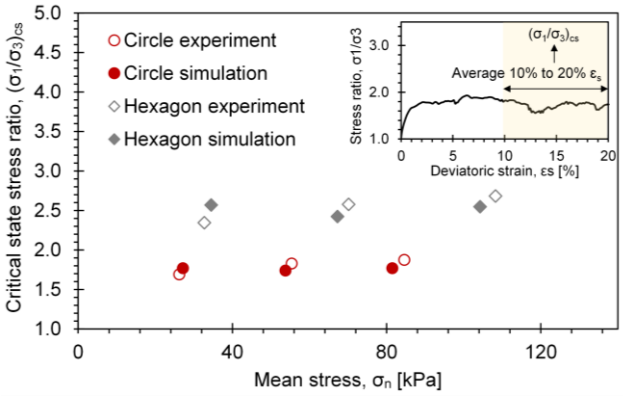

Figure 6. Relationship between mean stress (σ_n) and average critical state stress ratio $(\sigma_1/\sigma_3)_{cs}$ for different confining pressures for the case of simulations performed using detailed DEM model with actual particle shape (inset shows the definition of $(\sigma_1/\sigma_3)_{cs}$)

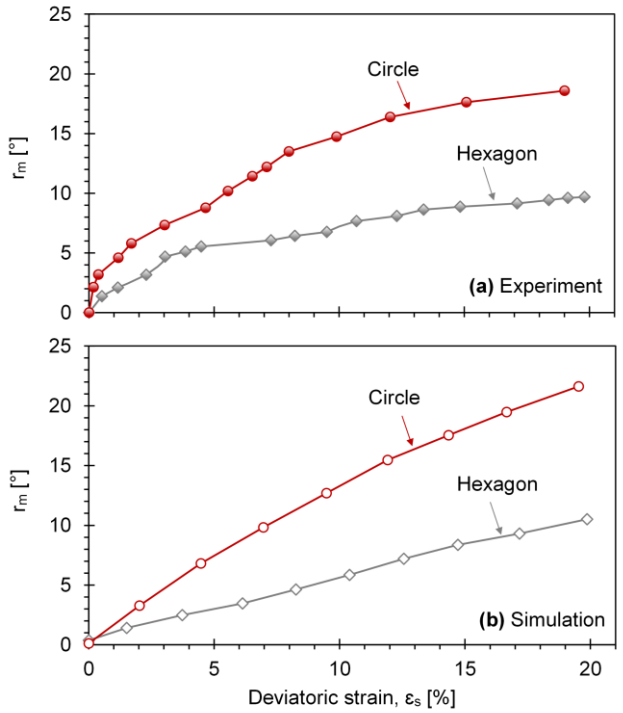

Figure 7. History of absolute average cumulative rotation (r_m) for complete assembly (σ_3=39.2 kPa) (a) experiment (b) simulation

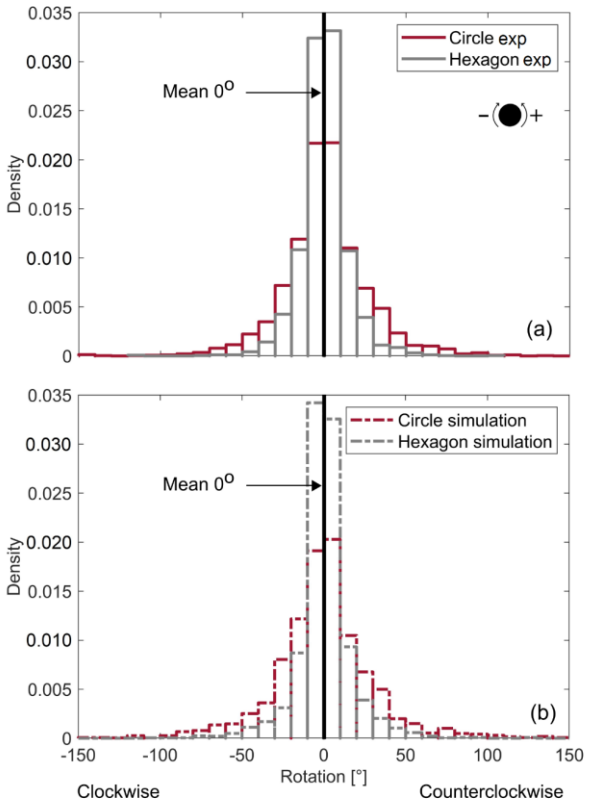

Figure 8. Histograms showing density distribution of cumulative rotation for each particle from initial to the final orientations during shearing (at $\varepsilon_s \approx 20$ % and σ_3=39.2 kPa) in (a) experiment (b) simulation

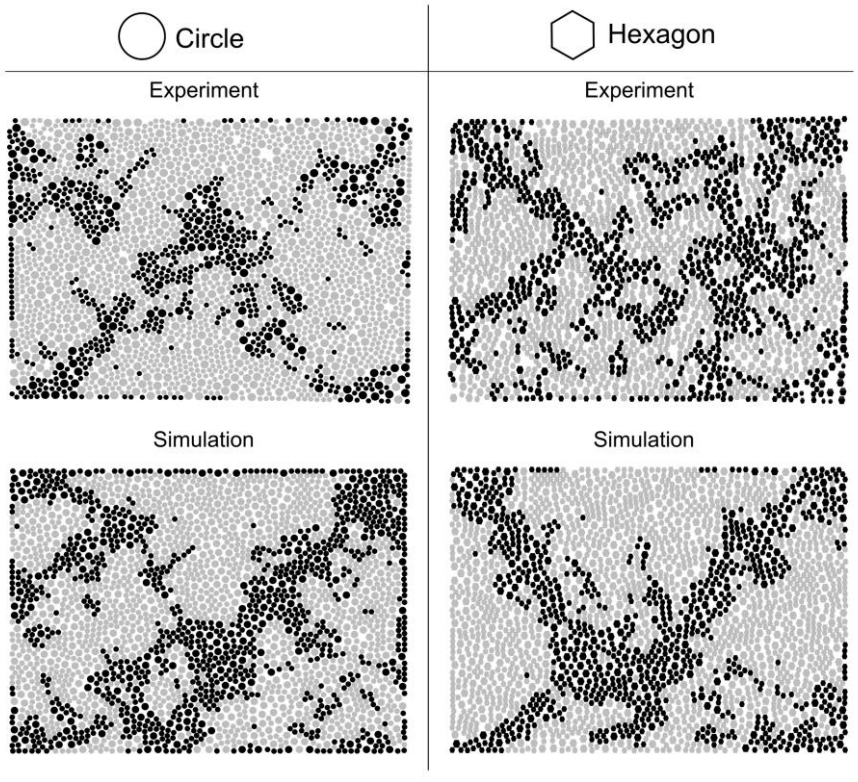

Figure 9. Shear band identification results. Black particles are assigned to the shear band (σ_3=39.2kPa)

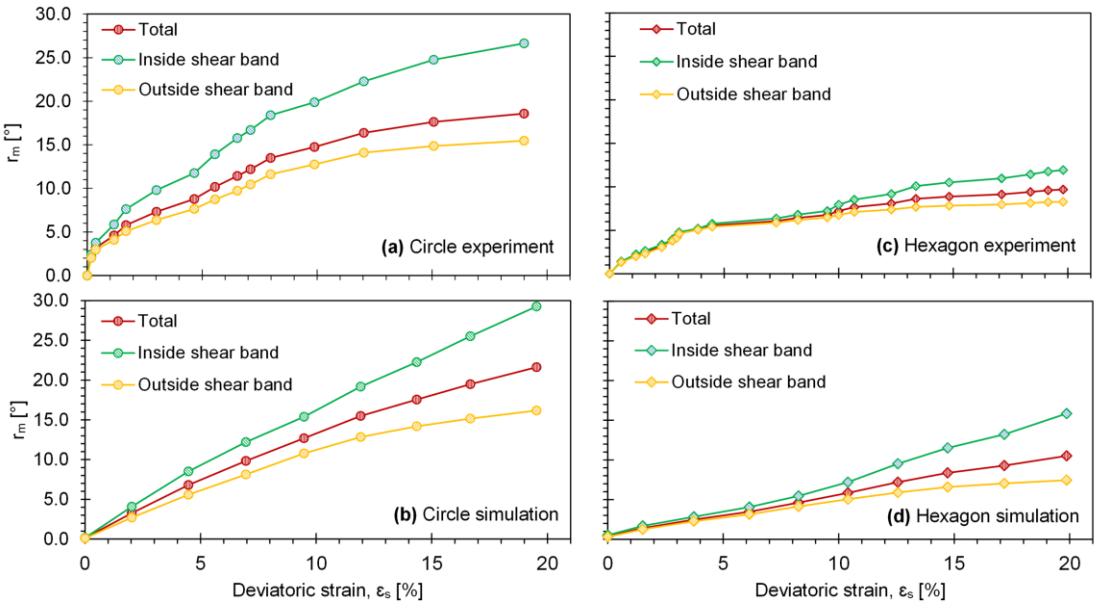

Figure 10. History of accumulated mean rotation inside and outside the shear band and for complete assembly (σ_3=39.2 kPa) (a) Circle experiment (b) Circle simulation (c) Hexagon experiment (d) Hexagon simulation

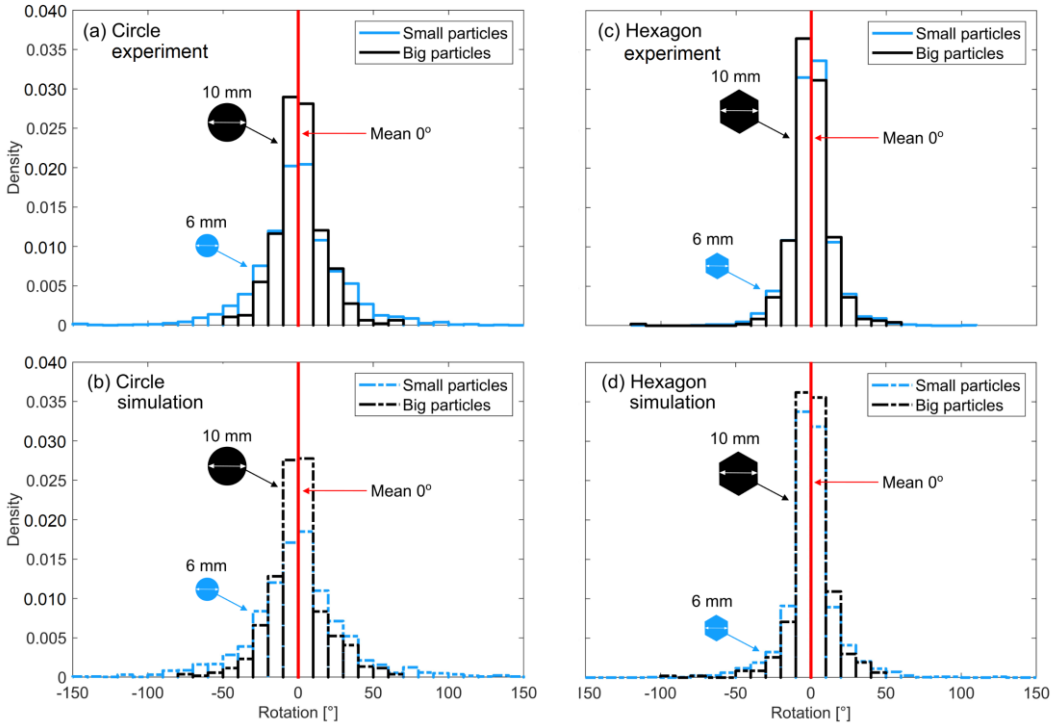

Figure 11. Histograms showing size-wise density distribution of cumulative rotation for each particle from initial to the final orientations during shearing (at $\varepsilon_s \approx 20$ % and σ_3=39.2 kPa) (a) experiment (b) DEM simulation.

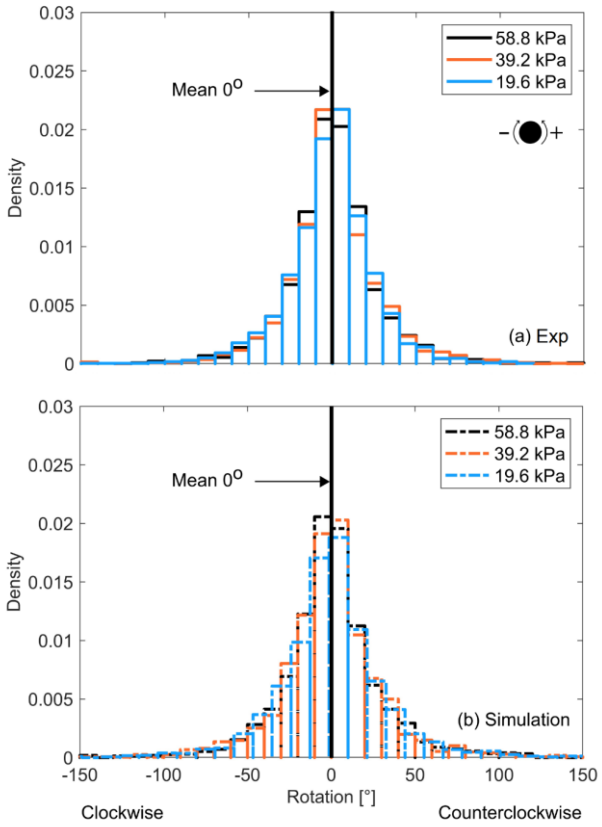

Figure 12. Histograms showing density distribution of cumulative rotation for each particle (circular) from initial to the final orientations during shearing at different confining pressures (at $\varepsilon_s \approx 20$ %) (a) experiment (b) DEM simulation.

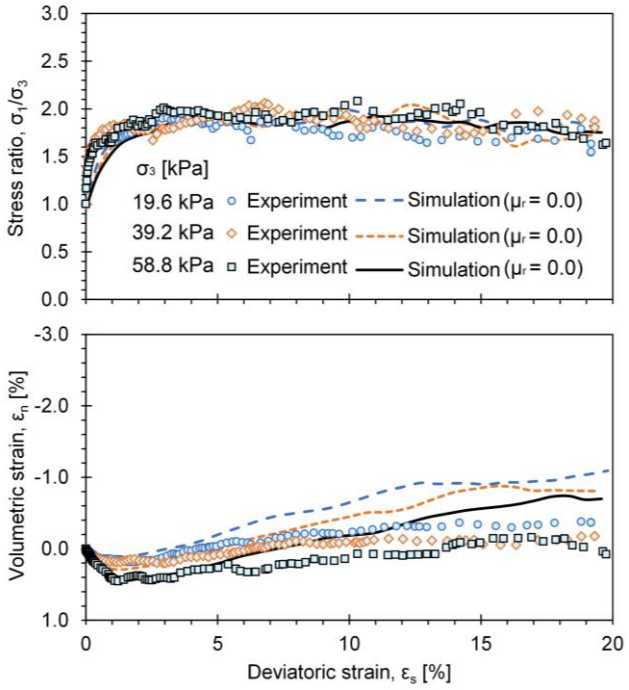

Figure 13. σ_1/σ_3 - ε_s and ε_n - ε_s relationships for circular particles observed in the experiment imitated by circular particles by applying rolling resistance linear contact model in simulation with $\mu_r = 0$

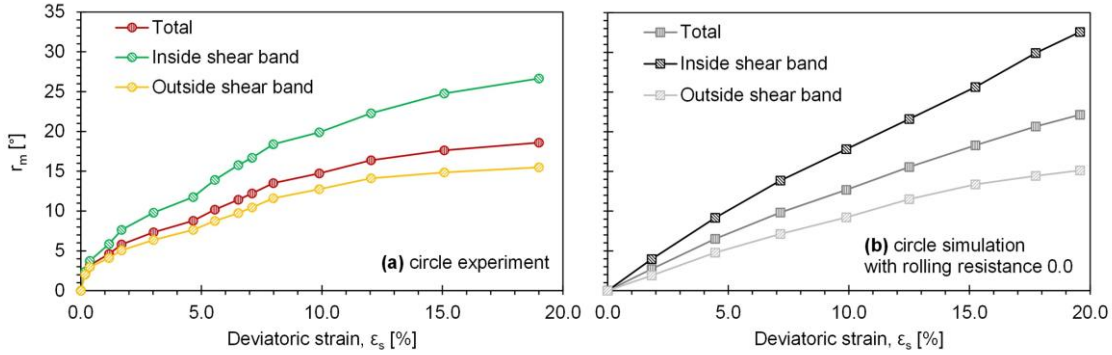

Figure 14. Comparison of particle rotations inside and outside shear band (a) experiment with circular particles (b) simulation with circular particles with rolling resistance linear contact model with $\mu_r = 0$ (σ_3=39.2 kPa)

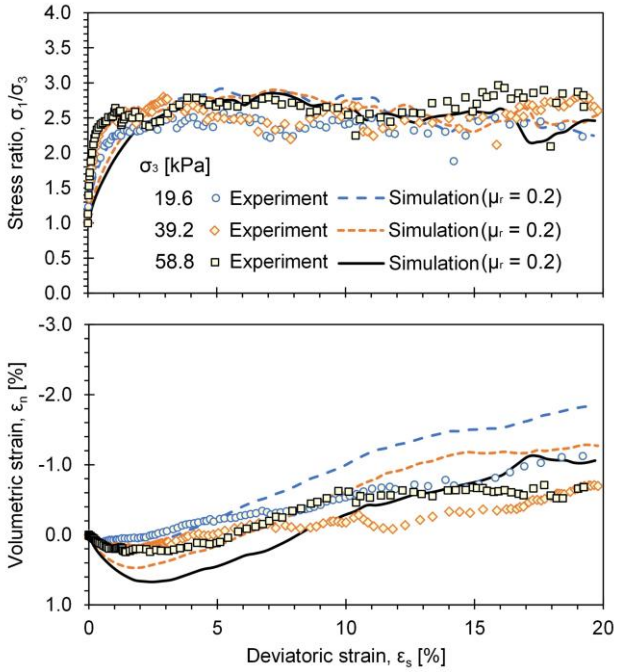

Figure 15. σ_1/σ_3 - ε_s and ε_n - ε_s relationships for hexagon particles observed in the experiment and imitated by circular particles by applying rolling resistance of 0.2 in simulation

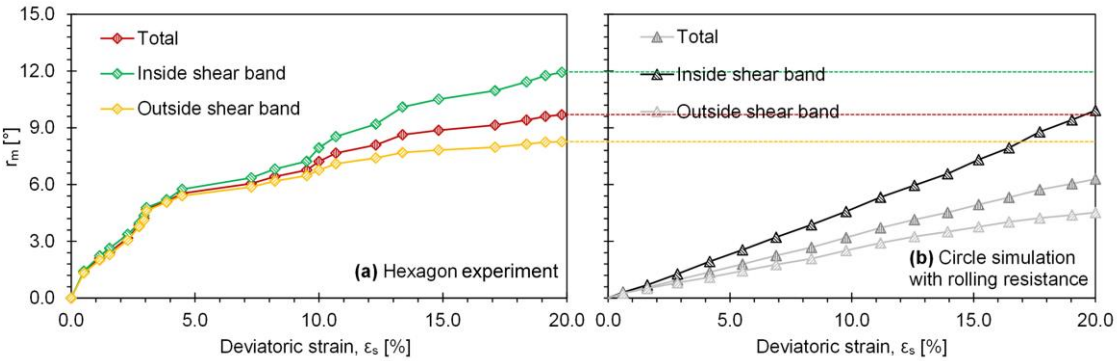

Figure 16. Comparison of particle rotations inside and outside shear band (a) experiment with hexagon particles (b) simulation with circular particles with rolling resistance of 0.2 (σ_3=39.2 kPa)

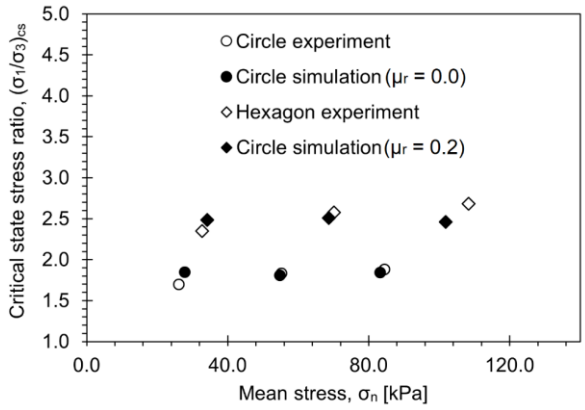

Figure 17. Relationship between mean stress (σ_n) and average critical state stress ratio $(\sigma_1/\sigma_3)_{cs}$ for different confining pressures for the case of simulations performed with simplified DEM model with rolling resistance

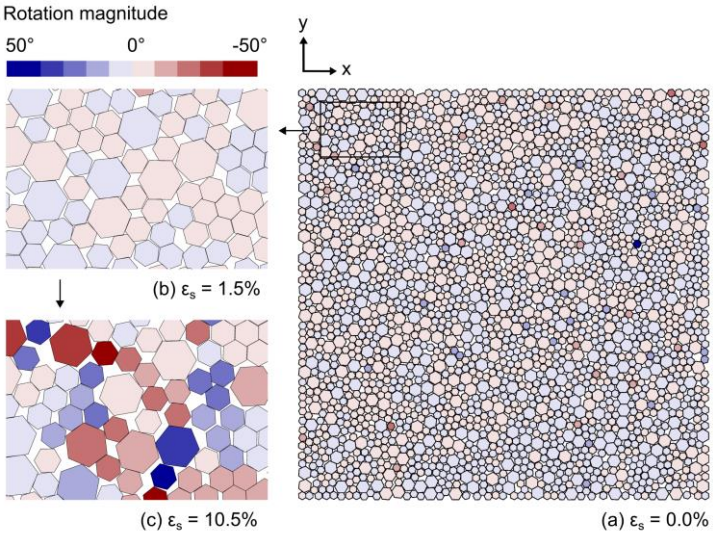

Figure 18. Evolution of particle arrangements (rotations) in hexagon (angular) assembly during shearing (σ_3 = 39.2 kPa)

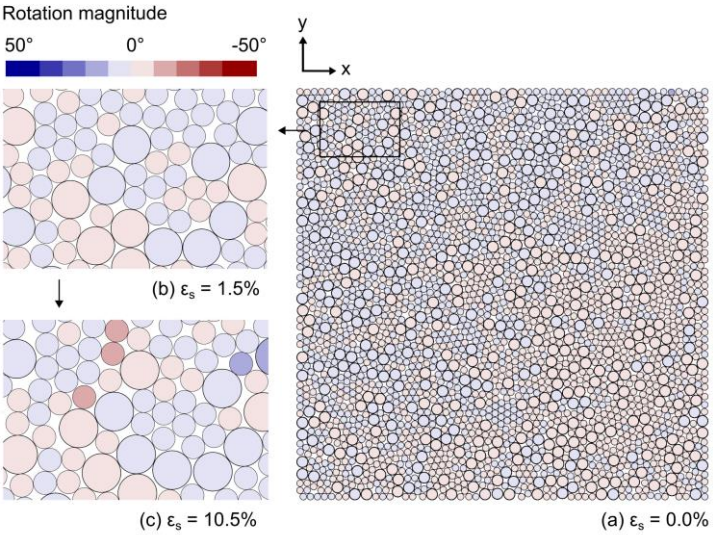

Figure 19. Evolution of particle arrangements (rotations) in circular (round) discs assembly with rolling resistance of 0.2 during shearing (σ_3 = 39.2 kPa)

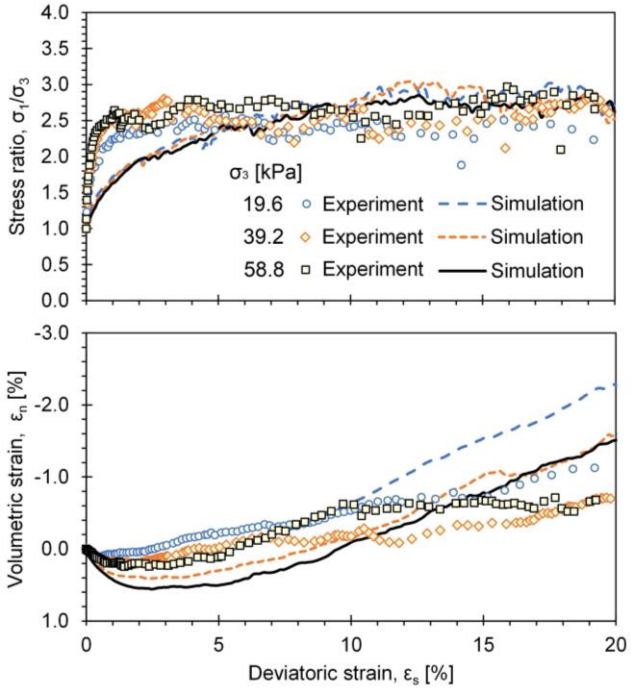

Figure A1. σ_1/σ_3 - ε_s and ε_n - ε_s relationships observed in experiment with hexagon particles and simulation with hexagonal particles with linear spring contact model

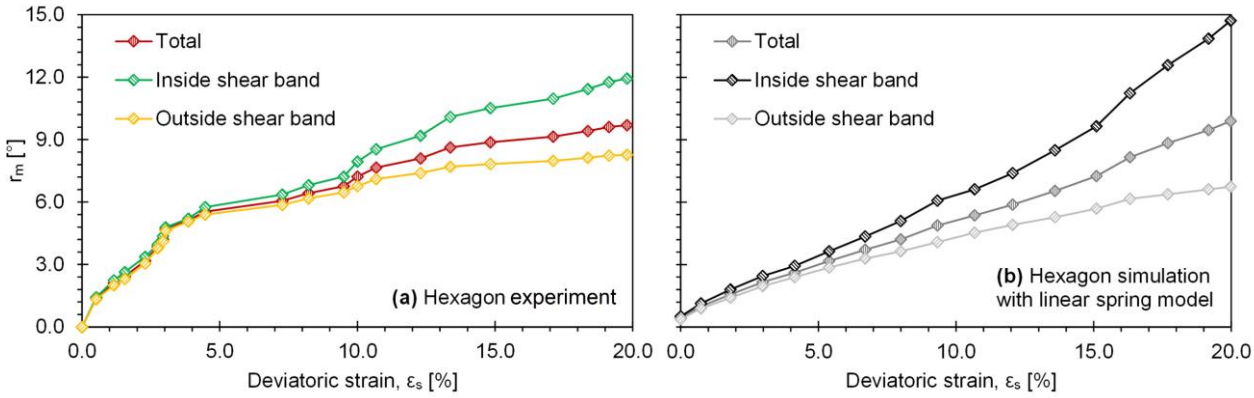

Figure A2. Comparison of particle rotations inside and outside shear band (a) experiment with hexagon particles (b) simulation with hexagonal particles with linear spring contact model (σ_3 = 39.2 kPa)

REFERENCES

Ali, U., M. Kikumoto, M. Ciantia, and Y. Cui. 2021. "Direct observation of particle kinematics in biaxial shearing test." *Proc. 18th UK Travelling Workshop, Geomechanics: from Micro to Macro*: 1-4. https://doi.org/10.20933/100001233.

Ali, U., M. Kikumoto, M. Ciantia, M. Previtali, and Y. Cui. 2023a. "Experimental micro–macromechanics: particle shape effect on the biaxial shear response of particulate systems." *Géotechnique*: 1–13. https://doi.org/10.1680/jgeot.22.00364.

Ali, U., M. Kikumoto, Y. Cui, M. Ciantia, and M. Previtali, 2023b. "Role of particle rotation in sheared granular media." *Acta*

Geotechnica 18: 4599–4614. https://doi.org/10.1007/s11440-023-01860-1.

Ali, U., M. Kikumoto, M. Ciantia, Y. Cui, and M. Previtali. 2023c. "Systematic effect of particle roundness/angularity on macro- and microscopic behavior of granular materials." *Granular Matter* 25 (3): 51. https://doi.org/10.1007/s10035-023-01341-y.

Ali, U., M. Kikumoto, and M. Ciantia. 2024. "Impact of particle elongation on the behavior of round and angular media: consequences of particle rotation and force chain development." *Computers and Geotechnics* 165: 105858. https://doi.org/10.1016/j.compgeo.2023.105858.

Andò, E., S. A. Hall, G. Viggiani, J. Desrues, and P. Bésuelle. 2012. "Grain-scale experimental investigation of localised deformation in sand: a discrete particle tracking approach." *Acta Geotechnica* 7 (1): 1–13. https://doi.org/10.1007/s11440-011-0151-6.

Azéma, E., N. Estrada, and F. Radjaï. 2012. "Nonlinear effects of particle shape angularity in sheared granular media." *Phys. Rev. E* 86 (4): 1–15. https://doi.org/10.1103/PhysRevE.86.041301.

Azéma, E., I. Preechawuttipong, and F. Radjai. 2016. "Binary mixtures of disks and elongated particles: texture and mechanical properties." *Phys. Rev. E* 94 (4): 1–12. https://doi.org/10.1103/PhysRevE.94.042901.

Azéma, E., and F. Radjaï. 2012. "Force chains and contact network topology in sheared packings of elongated particles." *Phys. Rev. E* 85 (3): 1–12. https://doi.org/10.1103/PhysRevE.85.031303.

Bardet, J. P. 1994. "Observations on the effects of particle rotations on the failure of idealized granular materials." *Mech. Mat.* 18 (2): 159–82. https://doi.org/10.1016/0167-6636(94)00006-9.

Bardet, J. P., and J. Proubet. 1991. "A numerical investigation of the structure of persistent shear bands in granular media." *Geotechnique* 41 (4): 599–613. https://doi.org/10.1680/geot.1991.41.4.599.

Binaree, T., E. Azéma, N. Estrada, M. Renouf, and I. Preechawuttipong. 2020. "Combined effects of contact friction and particle shape on strength properties and microstructure of sheared granular media." *Phys. Rev. E* 102 (2): 22901. https://doi.org/10.1103/PhysRevE.102.022901.

Binaree, T., I. Preechawuttipong, and E. Azéma. 2019. "Effects of particle shape mixture on strength and structure of sheared granular materials." *Phys. Rev. E* 100 (1): 1–10. https://doi.org/10.1103/PhysRevE.100.012904.

Catalano, E., B. Chareyre, and E. Barthélémy. 2014. "Pore-scale modeling of fluid-particles interaction and emerging poromechanical effects." *Int. J. Numer. Anal. Meth. Geomech.* 38 (1): 51–71. https://doi.org/10.1002/nag.2198.

Cavarretta, I., I. Rocchi, and M. R. Coop. 2011. "A new interparticle friction apparatus for granular materials." *Can. Geotech. J.* 48 (12): 1829–40. https://doi.org/10.1139/T11-077.

Chen, Z., M. Omidvar, K. Li, and M. Iskander. 2017. "Particle rotation of granular materials in plane strain." *Int. J. Phys. Modelling Geotech.* 17 (1): 23–40. https://doi.org/10.1680/jphmg.15.00046.

Ciantia, M. O., M. Arroyo, C. O'Sullivan, and A. Gens. 2019. "Micromechanical inspection of incremental behaviour of crushable soils." *Acta Geotechnica* 14 (5): 1337–56. https://doi.org/10.1007/s11440-019-00802-0.

Crocker, J. C., and D. G. Grier. 1996. "Methods of digital video microscopy for colloidal studies." *J. Colloid Interface Sci.* 179 (1): 298–310. https://doi.org/10.1006/jcis.1996.0217.

Cui, L., C. O'Sullivan, and S. O'Neill. 2007. "An analysis of the triaxial apparatus using a mixed boundary three-dimensional discrete element model." *Geotechnique* 57 (10): 831–44. https://doi.org/10.1680/geot.2007.57.10.831.

Cundall, P. A. 1979. "A discrete numerical model for granular assemblies." *Geeotechnique* 29 (1): 47–65. https://doi.org/10.1680/geot.1979.29.1.47.

Estrada, N., E. Azéma, F. Radjai, and A. Taboada. 2011. "Identification of rolling resistance as a shape parameter in sheared granular media." *Phys. Rev. E* 84 (1): 1–5. https://doi.org/10.1103/PhysRevE.84.011306.

Huang, J., M. Vicente da Silva, and K. Krabbenhoft. 2013. "Three-dimensional granular contact dynamics with rolling resistance." *Computers and Geotechnics* 49: 289–98. https://doi.org/10.1016/j.compgeo.2012.08.007.

Huang, X., K. J. Hanley, C. O'Sullivan, and C. Y. Kwok. 2014. "Exploring the influence of interparticle friction on critical state behaviour using DEM." *Int. J. Numer. Anal. Meth. Geomech.* 38 (12): 1276–97. https://doi.org/10.1002/nag.2259.

Huo, Y.X., Y.F. Leung, and C.Y. Kwok. 2023. "Micro-Mechanical Perspective on the Role of Particle Shape in Shearing of Sands." *Canadian Geotechnical Journal* 60 (10): 1515–31. https://doi.org/10.1139/cgj-2022-0270.

Iwashita, K., and M. Oda. 1998. "Rolling resistance at contacts in simulation of shear band." *J. Eng. Mech.* 124 (March): 285–92. https://doi.org/10.1061/(ASCE)0733-9399(1998)124:3(285).

Kawamoto, R., E. Andò, G. Viggiani, and J. E. Andrade. 2018. "All you need is shape: predicting shear banding in sand with LS-DEM." *J. Mech. Phys. Solids* 111 (Feb): 375–92. https://doi.org/10.1016/j.jmps.2017.10.003.

Kuhn, M. R., and K. Bagi. 2002. "Particle rotations in granular materials." In *Proc. 15th ASCE Eng. Mech. Conf.* 6.

Kuhn, M. R. 1999. “Structured deformation in granular materials.” *Mech. Mat.* 31 (6): 407–29. https://doi.org/10.1016/S0167-6636(99)00010-1.

Liu, Y., X. Liu, and W. Hu. 2023. “Competition mechanism between dilation and interlocking in granular soils: dem simulation and constitutive modeling.” *Acta Geotechnica* 18 (1): 149–69. https://doi.org/10.1007/s11440-022-01552-2.

Mindlin, R. D., and H. Deresiewicz. 1953. “Elastic spheres in contact under varying oblique forces.” *J. Appl. Mech.* 20 (3): 327–44. https://doi.org/10.1115/1.4010702.

Mirghasemi, A. A., L. Rothenburg, and E. L. Matyas. 2002. “Influence of particle shape on engineering properties of assemblies of two-dimensional polygon-shaped particles.” *Geotechnique* 52 (3): 209–17. https://doi.org/10.1680/geot.2002.52.3.209.

Misra, A., and H. Jiang. 1997. “Measured kinematic fields in the biaxial shear of granular materials.” *Computers and Geotechnics* 20 (3–4): 267–85. https://doi.org/10.1016/s0266-352x(97)00006-2.

Mitchell, J. K., and K. Soga. 2005. *Fundamentals of soil behavior*. 3rd ed. New Jersey: John Wiley & Sons, Inc.

Nie, Z., C. Fang, J. Gong, and Z. Liang. 2020. “DEM study on the effect of roundness on the shear behaviour of granular materials.” *Comp. Geotech.* 121 (May 2020): 103457. https://doi.org/10.1016/j.compgeo.2020.103457.

Nitka, M., and A. Grabowski. 2021. “Shear band evolution phenomena in direct shear test modelled with DEM.” *Pow. Tech.* 391: 369–84. https://doi.org/10.1016/j.powtec.2021.06.025.

Oda, M., J. Konishi, and S. Nemat-Nasser. 1982. “Experimental micromechanical evaluation of strength of granular materials: effects of particle rolling.” *Mech. Mat.* 1 (4): 269–283. https://doi.org/10.1016/0167-6636(82)90027-8.

Rorato, R., M. Arroyo, A. Gens, E. Andò, and G. Viggiani. 2021. “Image-based calibration of rolling resistance in discrete element models of sand.” *Comp. Geotech.* 131 (Jan): 103929. https://doi.org/10.1016/j.compgeo.2020.103929.

Rorato, R., M. Arroyo, E. Andò, A. Gens, and G. Viggiani. 2020. “Linking shape and rotation of grains during triaxial compression of sand.” *Granular Matter* 22 (4): 1–21. https://doi.org/10.1007/s10035-020-01058-2.

Rothenburg, L., and R. J. Bathurst. 1992. “Micromechanical features of granular assemblies with planar elliptical particles.” *Geotechnique* 42 (1): 79–95. https://doi.org/10.1680/geot.1992.42.1.79.

Schneebeli, M. 1956. “Une analogie mechanique pour les terres sans cohesion.” *Compte Rendus des Seances de l’Academie des Sciences* 243: 125–26.

Shin, H., and J. C. Santamarina. 2013. “Role of particle angularity on the mechanical behavior of granular mixtures.” *J. Geotech. Geoenviron. Eng.* 139 (2): 353–55. https://doi.org/10.1061/(asce)gt.1943-5606.0000768.

Smilauer, V., E. Catalano, B. Chareyre, S. Dorofeenko, and C. Jakob. 2015. “Yade documentation 2nd ed.” https ://doi.org/10.5281/zenodo.34073.

Tong, Z. X., L. W. Zhang, and M. Zhou. 2013. “DEM simulation of biaxial compression experiments of inherently anisotropic granular materials and the boundary effects.” *J. Appl. Math.* 2013. https://doi.org/10.1155/2013/394372.

Vallejo, L. E. 2001. “Interpretation of the limits in shear strength in binary granular mixtures.” *Can. Geotech. J.* 38 (5): 1097–1104. https://doi.org/10.1139/cgj-38-5-1097.

Wensrich, C. M., A. Katterfeld, and D. Sugo. 2014. “Characterisation of the effects of particle shape using a normalised contact eccentricity.” *Granular Matter* 16 (3): 327–37. https://doi.org/10.1007/s10035-013-0465-1.

Wu, K., S. Liu, W. Sun, and S. Rémond. 2020. “DEM study of the shear behavior and formation of shear band in biaxial test.” *Ad. Pow. Tech.* 31 (4): 1431–40. https://doi.org/10.1016/j.apt.2020.01.016.

Wu, M., F. Wu, and J. Wang. 2022. “Particle shape effect on the shear banding in DEM-simulated sands.” *Granular Matter* 24 (2): 1–17. https://doi.org/10.1007/s10035-022-01210-0.

Wu, M., L. Xiong, and J. Wang. 2021. “DEM study on effect of particle roundness on biaxial shearing of sand.” *Underground Space* 6 (6): 678–94. https://doi.org/10.1016/j.undsp.2021.03.006.

Yimsiri, S., and K. Soga. 2010. “Dem analysis of soil fabric effects on behaviour of sand.” *Geotechnique* 60 (6): 483–95. https://doi.org/10.1680/geot.2010.60.6.483.

Zhang, W., J. Wang, and M. Jiang. 2013. “DEM-aided discovery of the relationship between energy dissipation and shear band formation considering the effects of particle rolling resistance.” *J. Geotech. Geoenviron. Eng.* 139 (9): 1512–27. https://doi.org/10.1061/(asce)gt.1943-5606.0000890.

Zhao, S., X. Zhou, and W. Liu. 2015. “Discrete element simulations of direct shear tests with particle angularity effect.” *Granular Matter* 17 (6): 793–806. https://doi.org/10.1007/s10035-015-0593-x.